Bonding and physical properties of the scheelite-type materials $AgReO_4$ and $NaReO_4$

J. Spitaler* and Claudia Ambrosch-Draxl
Institut für Theoretische Physik, University Graz, Universitätsplatz 5, A-8010 Graz, Austria

E. Nachbaur and F. Belaj
Institut für Chemie, University Graz, Schubertstraße 1, A-8010 Graz, Austria

H. Gomm and F. Netzer
Institut für Experimentalphysik, University Graz, Universitätsplatz 5, A-8010 Graz, Austria
(Received 30 September 2002; published 27 March 2003)

The scheelite-type salts $AgReO_4$ and $NaReO_4$ are investigated by first-principles calculations based on density-functional theory. We calculate structural and vibrational properties as a function of pressure and analyze the electronic bands and charge densities in terms of the binding mechanism. We conclude that both compounds exhibit ionic bonding. Our studies are supplemented by x-ray-diffraction and x-ray photoelectron spectroscopy experiments. All theoretical results excellently agree with measured data.

DOI: 10.1103/PhysRevB.67.115127 PACS number(s): 71.20.−b, 31.10.+z, 82.80.Pv, 87.64.Bx

I. INTRODUCTION

Silver salts show typical ionic features similar to those of alkali-metal salts, e.g., Madelung energy, medium large band gaps, electric conductivity in solid and molten states, small lattice constants, but also many peculiar properties that clearly distinguish them from alkali-metal salts. The latter include the failure of the additivity rule of ionic radii, color phenomena, large lattice energies, a large dielectric constant, a low solubility in water, the predominance of Frenkel defects, high mobilities of interstitial silver ions, and peculiarities among their elastic constants and phonon spectra. Therefore, the nature of the chemical bonding in silver salt crystals is an issue of considerable interest. Since 1933 when the first set of interaction potentials for silver compounds was proposed by Mayer,[1] numerous experimental and theoretical studies concerning the bonding situation in silver compounds have been undertaken. While able to simulate some selected features, these models fall short of providing a consistent explanation of the cohesion properties in silver salts. Therefore, different opinions concerning this problem have been presented in the literature: (i) The bonding situation in silver salts is consistent with a fully ionic model, but could be equally well interpreted as indicating partial covalent bonding.[2–7] (ii) Essential contributions to the interionic forces in silver salts result from interactions between higher electric multipoles.[8–11] (iii) The peculiar properties of silver salts result from a dominance of strong van der Waals interaction over short-range repulsion.[12–14]

This ambiguous situation needs clarification where some very fundamental questions concerning the electronic properties of silver compounds have to be answered. In order to address these questions the electronic and lattice properties of $AgReO_4$ and $NaReO_4$, two representative compounds, which demonstrate nearly identical crystallographic data, are investigated in the framework of density-functional theory. These calculations are supplemented by x-ray-diffraction experiments for $AgReO_4$ and by x-ray photoelectron spectroscopy (XPS) measurements of both compounds.

II. COMPUTATIONAL DETAILS

All calculations were performed with the linearized augmented plane-wave (LAPW) technique utilizing the WIEN97 code.[15] Exchange and correlation effects were treated within the local-density approximation (LDA) using the form of Perdew and Wang.[16] For the semicore states Re $5s$ and $5p$, Ag $4s$ and $4p$, Na $2s$ and $2p$, and O $2s$, the LAPW basis set has been extended by local orbitals. The Re $4f$ electrons have been treated in two different ways. In one set of calculations, they were considered as core electrons, in the other one as valence states. In both cases calculations were performed for four different volumes of $NaReO_4$ and $AgReO_4$, respectively, thereby relaxing the oxygen coordinates. The results did not show any significant difference, neither in the energy dependence of the volume, nor in the bond length or density of states. Therefore the $4f$ electrons were treated as valence states in all further calculations, except for the computation of the x-ray near-edge emission spectra. The muffin-tin radii R_{MT} for Re and O were chosen 1.81 a.u. (0.96 Å) and 1.36 a.u. (0.72 Å), respectively, where the sum of both is only slightly smaller than the Re-O bond length. For the silver and sodium ions, atomic sphere radii of 2.0 a.u. (1.06 Å) and 1.6 a.u. (0.85 Å) were used, respectively. The plane-wave cutoffs G_{max} for expanding density and potential in the interstitial region were chosen to be 12 a.u.$^{-1}$ (22.68 Å^{-1}). The cutoff in the expansion of the wave functions into LAPW's K_{max} was 5.15 a.u.$^{-1}$ (9.73 Å)$^{-1}$), which corresponds to an $R_{mt}\,K_{max}$ value of 7.0 for oxygen, 9.3 for Re, 8.2 for Na, and 10.3 for Ag. The maximum l value for partial waves inside the atomic spheres was 10, and for the non-muffin-tin matrix elements a maximum of 4 was used. For all self-consistent field (SCF) calculations, a **k**-point sampling with 12 irreducible points of the Brillouin zone turned out to be sufficient, while the density of states (DOS) calculations were performed with a uniform **k** mesh of 143 irreducible points. In both cases the modified tetrahedron method[17] was applied for the **k** space integrations.

The convergence criterion for the SCF calculations was

the minimization of the force acting on the oxygen atom, with a convergence tolerance of 1 mRy/a.u. (1.89 mRy/Å). To obtain the Raman frequencies of $AgReO_4$ and $NaReO_4$, six additional configurations were computed for each structure, with the O atoms displaced by ± 0.02 a.u. (0.011 Å) in *x*, *y*, and *z* direction, respectively. The resulting data, together with oxygen coordinates [displacements up to 0.04 a.u. (0.021 Å)] and forces [values up to 20 mRy/a.u. (37.8 mRy/Å)] from the geometry-relaxation procedure, were used to set up the dynamical matrix and henceforth obtain the eigenmodes.

III. EXPERIMENT

A. Crystal structure

The x-ray-diffraction measurements were performed using graphite-monochromized Mo-K_α radiation at 95 K and 298 K. At the more precise low-temperature determination a total of 1062 reflections were collected (with a maximum angle Θ of 30°), from which 247 were unique ($R_{int} = 0.0380$). The structure was solved by direct methods (SHELXS-97) Ref. 18 and refined by full-matrix least-squares techniques against F^2 (SHELXL-97).[19] For 15 parameters final *R* indices of $R = 0.0185$ and $wR^2 = 0.0473$ (GOF = 1.153) were obtained.

B. X-ray photoelectron spectroscopy

The XPS experiments were carried out with a PHI 5400 electron spectrometer using unmonochromated Al-K_α radiation (1486.6 eV). The instrumental resolution is estimated to be 1.0 eV for survey scans and 0.8 eV for the C 1*s* line. The vacuum system, which was equipped with a load lock such that the sample could be introduced into vacuum without being baked, had a base pressure in the low 10^{-10}-mbar range. Samples were the purest obtainable from commercial suppliers [sodium perrhenate, 99.99%, $NaReO_4$, Aldrich; silver perrhenate, 98+%, $AgReO_4$, Alfa; polyethylene for spectroscopy, uvasol, $(CH_2)_n$, Merck] and are found to be stable upon x-ray irradiation from control experiments. For XPS measurements, the well ground powder samples were mixed with polyethylene in an agate mortar. Finally, the sample was placed onto a fritted stainless steel plate ($\emptyset = 1/2$ in, Supelco) situated inside an evacuable KBr die (Perkin-Elmer) and a clear disk was pressed in a hydraulic press (Perkin-Elmer) to form a polyethylene pellet fixed on the frit, which was mounted to the sample holder using a double-sided conducting adhesive tape. To correct the static charge effect, which is critical for nonconducting samples, we used two internal energy references: the Ag $3d_{5/2}$ energy level fixed at 368.0 eV, and the Re $4f_{7/2}$ energy level fixed at 46.1 eV. According to the literature[20–23] these binding energies are stable for a significant number of related compounds.

By combining the point-charge electrostatic model proposed by Citrin[24] with qualitative intensity considerations, it was possible to make an unambiguous assignment of the photoemission spectra for $AgReO_4$ and $NaReO_4$.

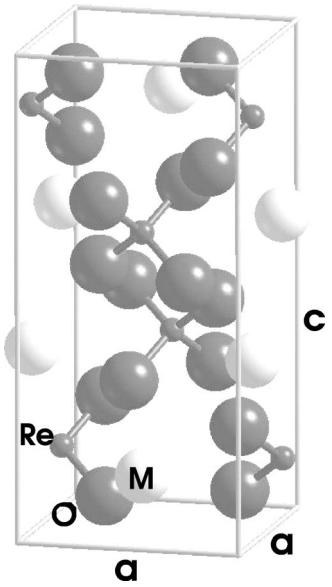

FIG. 1. Unit cell of $MReO_4$ with $M = (Na, Ag)$.

IV. RESULTS

A. Structural properties

Both $AgReO_4$ and $NaReO_4$,[26,25] crystallize in the scheelite-type tetragonal structure with the space group $I4_1/a$. It consists of ReO_4 tetrahedra, connected by MO_8 ($M = Na, Ag$) dodecahedra, respectively. Rhenium and silver (sodium) occupy high-symmetry positions with site symmetry $4a$ and $4b$ and the coordinates $(0, \frac{1}{4}, \frac{1}{8})$ and $(\frac{1}{2}, \frac{3}{4}, \frac{1}{8})$, respectively. The only internal degrees of freedom are the oxygen coordinates (site symmetry $16f$). The unit cell of $MReO_4$ is depicted in Fig. 1.

The lattice parameters of $AgReO_4$ measured at two different temperatures are summarized in Table I together with literature data for $AgReO_4$ and $NaReO_4$. The temperature effect between 95 and 298 K is 1%, where the room-temperature data agree very well with measurements carried out by Naumov *et al.*[27] The unit-cell volumes of $AgReO_4$ and $NaReO_4$ taken at room temperature differ by 0.9% only, although Ag^+ ions have 46 electrons compared to 10 electrons of Na^+. This surprising fact will be investigated now theoretically. To this extent the total energy was calculated as a function of the unit-cell volume. This procedure allows to determine the equilibrium volume and to study pressure effects at the same time. In a first step, the volume was optimized for a fixed axes ratio thereby relaxing the oxygen coordinates.

TABLE I. Structural parameters of $AgReO_4$ compared to literature data[27] and measurements for $NaReO_4$(Ref. 25)

	a (Å)	*c* (Å)	*V*(Å^3)	*T* (K)	Ref.
$AgReO_4$	5.3585	11.722	336.58	95	
	5.3742	11.792	340.6	298	
	5.372	11.793	340.4	297	27
$NaReO_4$	5.3654	11.732	337.49	296	25

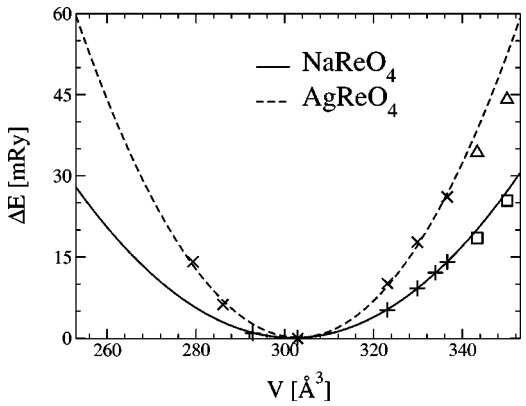

FIG. 2. Total energy of $NaReO_4$ and $AgReO_4$ as a function of volume. The lines indicate fits through the data points marked by crosses. The open symbols correspond to data points outside the harmonic range. For all points the oxygen coordinates have been relaxed.

In Fig. 2, the total energy of both compounds is shown as a function of volume where the energies of the corresponding optimal volumes were taken as reference energies. Within a wide range the energy decrease is quadratic in the volume. Deviation from this behavior at very large cell dimensions can be made out by the data points indicated by open triangles for $AgReO_4$ and squares for $NaReO_4$. Theoretically the energy minimum of $AgReO_4$ ($NaReO_4$) is found at 90.1% (89.7%) of the experimental volume. This 10% deviation from experiment is due to the well-known overbinding effect of the local-density approximation.[28] The optimized values of $AgReO_4$ and $NaReO_4$ differ by 0.1% only which is in excellent agreement with experiment and a good starting point for the interpretation of the bonding mechanism in these compounds.

In Table II, the structural data as obtained from our LAPW calculations for different cell volumes are summarized and compared to available literature data for ambient pressure. It shows that in both compounds the relative coordinates of the oxygen atom change systematically as a function of volume, but the Re-O distance stays the same. This incompressibility of the ReO_4 tetrahedra is in excellent agreement with experimental Raman data obtained for $AgReO_4$.[29]

In a next step of our theoretical investigations, the axes ratios of $NaReO_4$ have been varied. The force-free position of the oxygen atoms has been searched for again in each configuration. The resulting data are given in Table III. There is a trend of increasing c/a ratio for smaller volumes. This indicates a different compressibility of $NaReO_4$ in c direction

TABLE III. Structural data of $NaReO_4$ for different unit-cell volumes obtained by a full geometry optimization, i.e., when the total energy is minimized with respect to the c/a ratio and the oxygen coordinates.

V/V_{expt} (%)	c/a	x (a)	y (a)	z (c)	d(Re-O) (Å)
99.7	2.1876	0.2291	0.1158	0.0402	1.736
98.9	2.1657	0.2311	0.1153	0.0408	1.736
95.7	2.1438	0.2332	0.1127	0.0400	1.736

TABLE II. Theoretically obtained structural data for $NaReO_4$ and $AgReO_4$ compared to experiment. x,y,z are the coordinates of the oxygen atom.

	V(Å^3)	V/V_{expt} (%)	x (a)	y (a)	z (c)	d (Re-O) (Å)	$d(M$-O) (Å)
$AgReO_4$							
Expt.	336.58	100.0	0.2314	0.1160	0.0409	1.739	2.524
Expt. (Ref. 27)	340.6	101.2	0.2306	0.1178	0.0419	1.727	2.625
Theory	350.052	104	0.2258	0.1110	0.0421	1.744	2.593
	343.320	102	0.2271	0.1099	0.0416	1.744	2.569
	336.586	100	0.2292	0.1089	0.0414	1.744	2.546
	329.854	98	0.2339	0.1135	0.0400	1.749	2.495
	323.122	96	0.2342	0.1094	0.0397	1.749	2.480
	302.927	90	0.2345	0.0981	0.0388	1.744	2.437
	286.098	85	0.2380	0.0945	0.0370	1.743	2.372
	279.366	83	0.2387	0.0919	0.0362	1.743	2.349
$NaReO_4$							
Expt. (Ref. 25)	337.490	100.0	0.2327	0.1211	0.0420	1.728	2.582
Theory	350.052	103.7	0.2291	0.1206	0.0418	1.737	2.565
	343.320	101.7	0.2281	0.1159	0.0413	1.736	2.554
	336.586	99.7	0.2307	0.1161	0.0409	1.737	2.525
	333.893	98.9	0.2314	0.1158	0.0407	1.737	2.515
	329.851	97.7	0.2324	0.1154	0.0406	1.734	2.502
	323.122	95.7	0.2332	0.1127	0.0400	1.736	2.481
	302.927	89.8	0.2335	0.1000	0.0390	1.735	2.439
	292.830	86.8	0.2373	0.1002	0.0380	1.734	2.392

TABLE IV. A_{1g} Raman frequencies of $AgReO_4$ and $NaReO_4$ as obtained by theory compared to experimental results Refs. 29,33, and 38 for $AgReO_4$.

$V(Å^3)$	$\omega_1(cm^{-1})$	$\omega_2(cm^{-1})$	$\omega_3(cm^{-1})$
$AgReO_4$			
336.6	934	313	169
302.9	925	318	184
279.4	923	333	233
Expt. (Ref. 29)	941	333	141
Expt. (Ref. 33)	943	330	
Expt. (Ref. 38)			132
$NaReO_4$			
336.6	977	326	152
302.9	977	335	172
292.8	983	343	190
Expt. (Ref. 33)	958	334	145

compared to the *a* axis. Even though there are no experimental data available for $NaReO_4$, this corresponds to the experimental findings for $AgReO_4$.[30] However, the energy gain by the optimization of the axes ratios turned out to be extremely small (0.44 mRy for $V=V_{exp}$), such that the optimum volume for $NaReO_4$ only changes from 89.68% to 89.51% of the experimental value. Therefore, the analogous calculations have not been performed for $AgReO_4$, and the structures with optimized oxygen positions have been taken as the starting points for all further investigations.

The bulk modulus B_0 of $NaReO_4$ obtained for the optimized volume by the second derivative of the total energy given in Fig. 2 is 18.3 GPa. Using the Burch-Murnaghan equation of state for a fit of the same points yields a value of 12.6 GPa for B_0 and -4.8 for its derivative B_0'. This discrepancy reflects the pressure dependence of B_0. For $AgReO_4$ the bulk modulus calculated from a harmonic fit of the total energies is 37.1 GPa, whereas the Burch-Murnaghan equation of state yields $B_0=30.38$ GPa and $B_0'=3.80$. Including more data points (marked by the open triangles in Fig. 2) yields a bigger B_0' of 6.1, indicating again a deviation from the harmonic behavior. B_0 is in good agreement with the experimental value of 30.9 ± 4 GPa.[30] The experimentally obtained B_0' was reported to be 30.9 ± 6. The much higher bulk modulus of $AgReO_4$ is consistent with findings of Schlosser[32] who investigated the quantity $B_0 d_{nn}^{3.5}$ with d_{nn} being the anion-cation distance for different halides. He reported 70% higher average values for Ag halides compared to Na halides. Since the anion-cation distances are the same in $NaReO_4$ and $AgReO_4$, a direct comparison of the bulk moduli allows for a similar conclusion for the perrhenates.

B. Phonons

The A_{1g} Raman frequencies for both compounds were calculated as a function of pressure and are presented in Table IV. For $NaReO_4$ the eigenfrequencies are found at 977 cm^{-1}, 326 cm^{-1}, and 152 cm^{-1}, respectively. All frequencies agree very well[31] with their experimental counterparts[33] of 958 cm^{-1}, 334 cm^{-1}, and 145 cm^{-1}, respectively, with deviations of a few wave numbers only. The corresponding eigenvectors are $(-0.72,0.40,0.56)$, $(0.55,-0.16,0.82)$, and $(-0.42,-0.90,0.10)$ with the components denoting the displacement of oxygen into *x*, *y*, and *z* direction, respectively. The first mode is a vibration of the oxygen atom towards its covalently bound Re neighbor which explains its high frequency. While this mode is hardly affected by pressure, the other two frequencies significantly increase with smaller volume. The eigenvectors, however, stay the same which can be attributed to the incompressibility of the Re-O bond as described above. The three unit-cell volumes taken into account theoretically refer to the experimental cell size (336.6 $Å^3$), the theoretically optimized volume (302.9 $Å^3$), and 83% of the experimental value (279.4 $Å^3$).

The A_{1g} Raman frequencies for $AgReO_4$, i.e., 934 cm^{-1}, 312 cm^{-1}, and 169 cm^{-1}, are also close to experiment, with the biggest deviation for ω_3. This mode is very sensitive to the unit-cell volume and thus strongly affected by pressure. This finding agrees very well with experimental observations. As reported in Ref. 29, the frequency of the 941-cm^{-1} mode is found to be almost unchanged under pressure with only a slight decrease, while the other two frequencies exhibit a significant increase under compression, which is 2.8 times larger for the mode smaller in frequency. This behavior is very well reproduced by theory, where the slopes between these two modes differ by a factor of 3.2. The eigenvectors at ambient pressure, $(-0.71,0.42,0.57)$, $(0.57,-0.13,0.81)$, and $(-0.42,-0.90,0.15)$, are nearly the same as for $NaReO_4$ with as little pressure effect.

C. Electronic Properties

The band structures of $NaReO_4$ and $AgReO_4$ are plotted along five symmetry directions in the Brillouin zone of the body-centered tetragonal lattice (Fig. 3, top right) for the experimental unit-cell volume. Within the LAPW method the band characters can be analyzed according to their atomic contributions inside the muffin-tin spheres, which are highlighted in the figure by the size of the circles. This analysis is presented for the Re *d* and the O *p* character for both compounds, and in addition for the Ag *d* character in $AgReO_4$. In the entire energy region shown in the plot no Na *s* states are present.

$NaReO_4$ is a direct band-gap material with the maximum of the valence band and the minimum of the conduction band at the Γ point. The LDA band gap is found to be 3.67 eV. The dispersion of the valence bands is relatively small and comparable in both the *a* and the *c* direction. The lowest region of the valence band between -5 eV and -3.5 eV has predominantly Re $5d$ (mainly $5d_{xz,yz}$) character, but still some O $2p$ admixture and is separated by a 0.4-eV gap from the lower pure O $2p$ band. The upper region of the valence band is formed by O $2p$ states. The conduction band has dominating Re $5d$ character together with some O $2p$ contribution. It splits up into two parts: The lower part of the conduction band is composed primarily by states associated with Re $5d_{z^2}$, Re $5d_{x^2-y^2}$ symmetry and O $2p$ states. It is separated by ≈ 1.2 eV from its upper part, which is formed

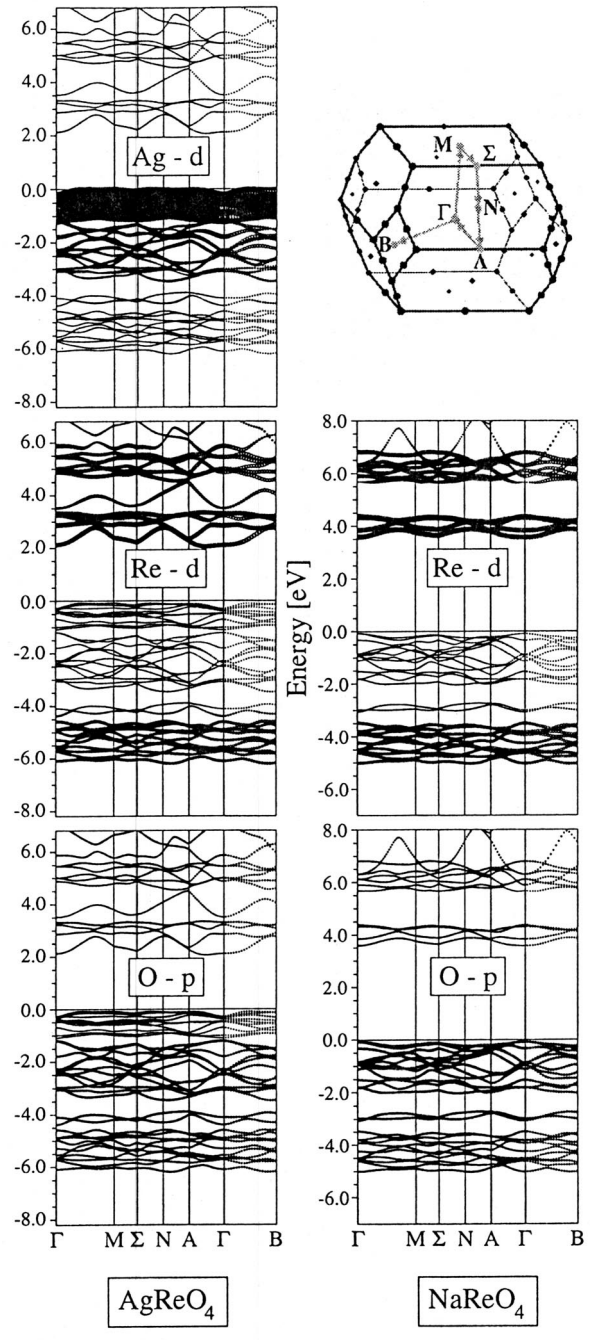

FIG. 3. Band structure of $AgReO_4$ (left panel) and $NaReO_4$ (right panel). The energy is given in eV with E_F taken as reference energy. The atomic band characters of Ag *d* (upper panel), Re *d* (middle panels), and O *p* (lower panels) are highlighted by the size of the circles. In the uppermost right panel, the Brillouin zone (BZ) of the body centered tetragonal cell is depicted.

by states of Re $5d_{xy}$ and $5d_{xz,yz}$ and O $2p$ character. Note that this decomposition of the *d* bands is done with respect to the Cartesian crystal axes, which are not the directions of the Re-O bonds.

In $AgReO_4$ the band extrema are not found at the Γ point, it exhibits an indirect band gap of 2.0 eV. The band structure is, however, extremely similar to that of $NaReO_4$ with the only significant difference being the Ag *d*-bands located just

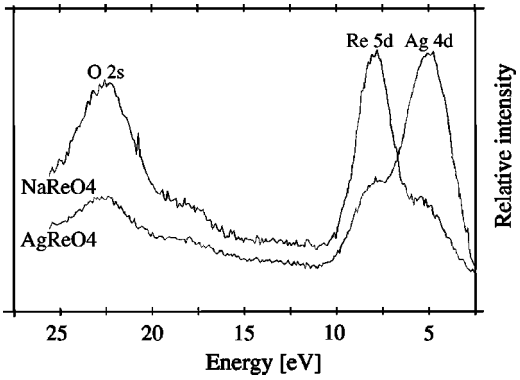

FIG. 4. Experimental XPS valence-band spectra for $NaReO_4$ and $AgReO_4$.

below the Fermi level. The *d*-band width thus determines the reduction of the band gap with respect to $NaReO_4$. A study for $CdMoO_4$ (Ref. 34) reveals a very similar situation with the same valence-band width, but the Cd *d* bands located below the MoO_4 valence states.

The fundamental band gap was determined for six different volumes of $AgReO_4$. It decreases linearly with decreasing pressure, with a slope of -112 meV per GPa. Although the LDA band gaps cannot be interpreted as the real gaps, the trend can be well compared to experimental findings. Experimentally, also a linear decrease was found with $dE/dP = -80$ meV per GPa.[30]

D. Spectroscopy

The calculated electronic structure can be probed by spectroscopic methods, where XPS valence-band spectra are directly proportional to the density of states. These two quantities are depicted in Figs. 4 and 5, respectively, in the investigated energy range of the valence band. The experimental spectra are normalized to the maximum intensity of the respective *d* bands. Therefore, only the relative peak heights within one spectrum can be compared, but not the absolute intensities between the spectra. Note that the experimental energy scale is referenced to the spectroscopic Fermi level, whereas the zero-point energy in the theoretical DOS is given by the highest occupied state for zero temperature. Therefore the absolute energy scales are not directly comparable.

Both the $NaReO_4$ and $AgReO_4$ samples show a feature at ~ 23 eV (O $2s$ region) and a doublet feature of equal width (~ 7.5 eV) on top of the valence band. For $NaReO_4$, the first photoelectron peak in the upper valence-band region corresponds to the nonbonding O $2p$ orbitals at ~ 6 eV and to the bonding Re $5d$–O $2p$ orbitals at ~ 8 eV. This is in good agreement with the theoretical findings for the DOS [Fig. 5(a)], which shows a Re like peak between -5 and -3.5 eV, and an oxygen related peak between -2 eV and the Fermi level, respectively.

For $AgReO_4$, the situation in the upper valence-band region has completely changed. The reversal of the intensity of the doublet feature is taken as evidence that the Ag $4d$ levels

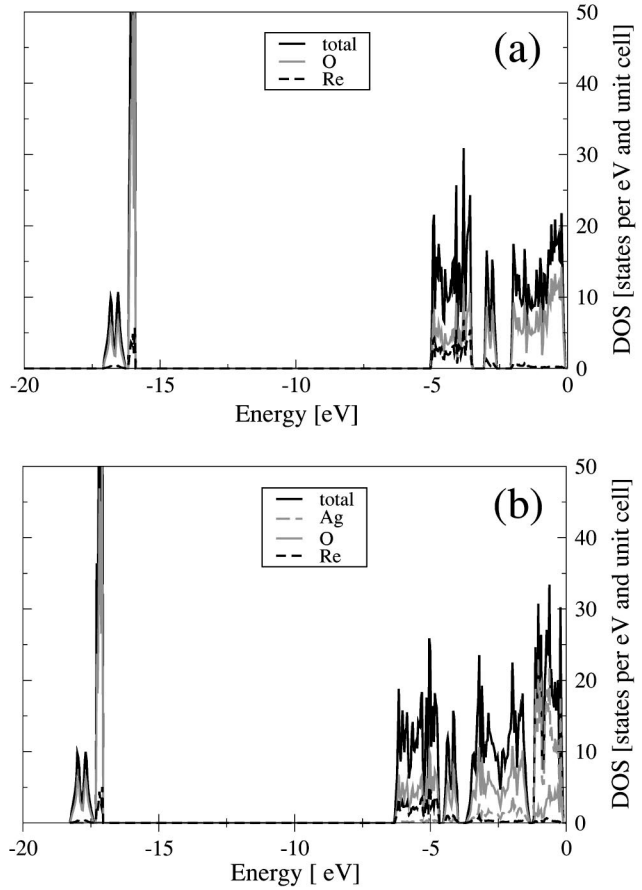

FIG. 5. Valence-band DOS of $NaReO_4$ (a) and $AgReO_4$ (b) as obtained by theory.

at ~5 eV form the topmost portion of the valence band in this compound followed by a less intense maximum at ~8 eV due to the bonding Re $5d$–O $2p$ states. The absence of the broad threshold feature associated with the nonbonding O $2p$ state ionization is only to a small extent the result of a superposition by the Ag $4d$ levels, but mainly due to the rigid shift of the valence bands to lower energies as found in the band structure. Thus the O $2p$ states are masked by the other states. Both the upper and lower peaks are perfectly reproduced by the corresponding features of the $AgReO_4$ valence-band DOS. Note that the spectra are given in arbitrary units. This means that the relative peak heights within each spectrum can be interpreted, but the magnitudes of the two curves cannot be compared with each other.

TABLE V. Binding energy (BE) in eV of different valence levels in $NaReO_4$ and $AgReO_4$.

Electron level	$NaReO_4$ BE (eV)	$AgReO_4$ BE (eV)
O $2s$	22.8	22.8
Re $5d$	8.1	8.1
O $2p$	5.7	n.o.
Ag $4d$		5.1
Re $4f_{7/2}$–Re $5d$	37.8	37.8
O $2s$–Re $5d$	14.7	14.7
O $2s$–O $2p$	17.1	

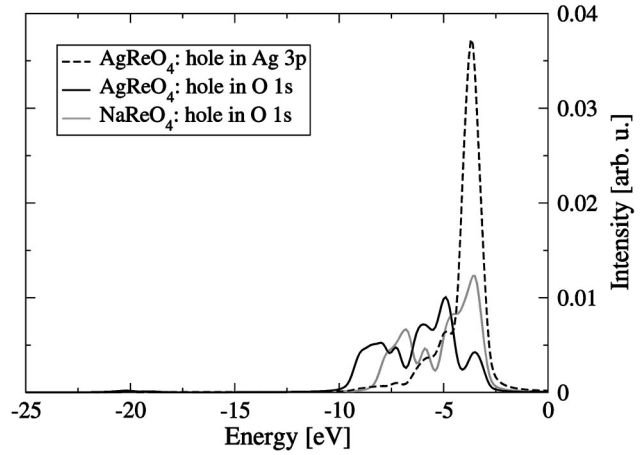

FIG. 6. Theoretical near-edge emission spectra for $NaReO_4$ ($AgReO_4$) with the core hole created in the O $1s$ (O $1s$, Ag $3p$) level.

The experimental binding energies of different valence levels in both compounds are summarized in Table V.

The near-edge structure of the x-ray emission spectra as obtained from theory is presented in Figs. 6 and 7. The spectra were calculated taking into account the dipole allowed transitions. Due to these selection rules only a limited number of different transitions is possible and deviations from the atomic dipole selection rules are an indication for a mixed atomic character of the electronic bands. Note that the zero point of the energy is arbitrarily chosen, therefore the peak postions are shifted with respect to the DOS.

In Fig. 6, the probability of transitions to the Ag $3p$ hole of $AgReO_4$ within the valence-band region is represented by the dashed curve. One pronounced and broad peak can be distinguished from smaller features at lower energies. Due to the selection rules, possible transitions are limited to Ag $4s$ and Ag $4d$ states, where only the latter ones lie in the considered energy range. Therefore this spectrum clearly reflects

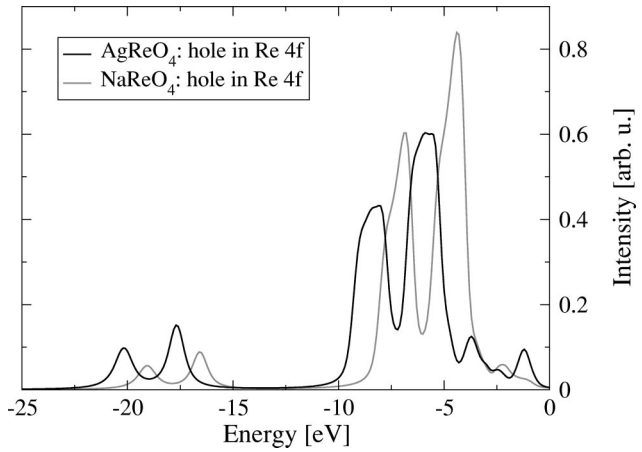

FIG. 7. Theoretical near-edge emission spectra for $NaReO_4$ and $AgReO_4$, when the hole is created in the Re $4f$ level.

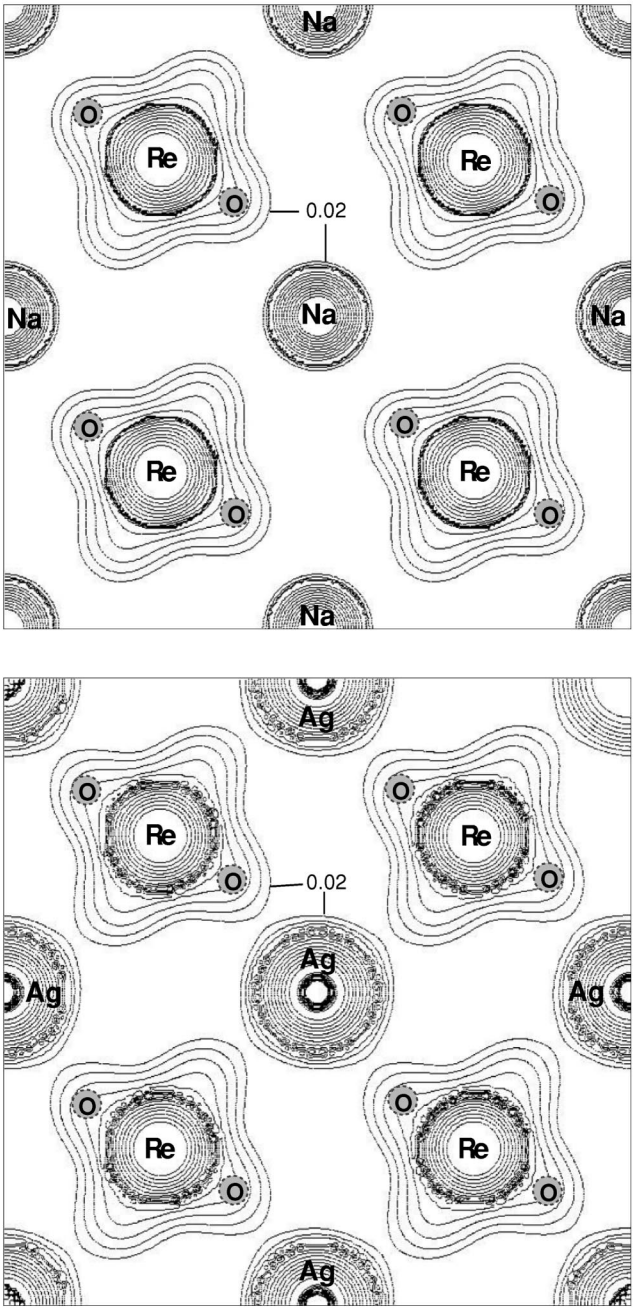

FIG. 8. Contour plot of the electron density in the M-Re plane of $NaReO_4$ (upper panel) and $AgReO_4$ (lower panel). The isolines range from 0.02 e/a.u.^{3} (0.13 e/Å^3) to 0.5 e/a.u.^{3} (3.37 e/Å^3) with a logarithmic increment. The Re-Re distance corresponds to the lattice parameter a. The O atoms lie approximately 1 Å above this plane.

the Ag valence DOS depicted in Fig. 5(b). The other lines represent the probability of transitions from higher-lying states to a hole in the O 1s level in $AgReO_4$ (black), and in $NaReO_4$ (gray), respectively. Since only transitions from O 2p states are possible, the intensity is proportional to the O 2p DOS. This is realized in Fig. 5(a) and the corresponding XPS results (Fig. 4), showing peaks for the O 2p bands in the same energy range. The shift of the $AgReO_4$ spectrum with respect to $NaReO_4$ indicates that in the latter compound

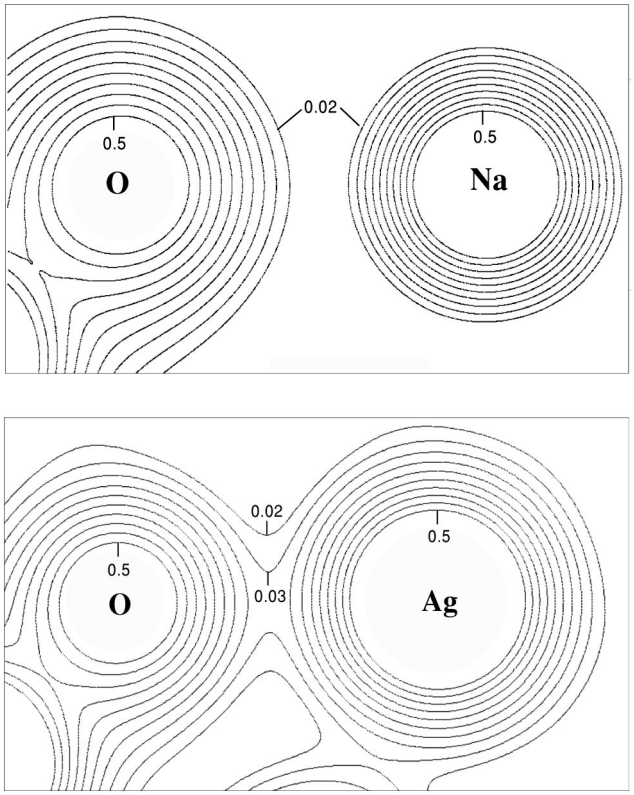

FIG. 9. Contour plot of the electron density in the M-O-Re plane of $NaReO_4$ (upper panel) and $AgReO_4$ (lower panel) where the M-O distance is the smallest. The isolines range from 0.02e/a.u.^{3} (0.13 e/Å^3) to 0.5 e/a.u.^{3} (3.37 e/Å^3) with a logarithmic increment.

the oxygen bands are lowered in energy due to the insertion of the Ag d bands. The first feature in the $AgReO_4$ spectrum reflects the small admixture of oxygen in the Re d bands as already found in the band structure.

When the hole is introduced in the Re 4f states, the spectra of the two compounds again differ by an energy shift as already found for the O 1s spectra. Both curves exhibit double peak structures in the region down to -10 eV as well as at low energies. The doubling of each feature has its origin in the splitting of the Re 4f core levels by 2.5 eV where the intensity ratio is determined by the occupation numbers of these states (8:6) . It is obvious from the DOS and the band structure that the spectra are governed by Re 5d states. This fact is again explained by the selection rules, prohibiting transitions from any other higher occupied state but Re 5d. The much higher intensity of the Re 4f spectra compared to those depicted in Fig. 6 is related to the larger amount of both final and initial states (4f,5d). In contrast to the Re 4f case, such a double-peak structure is not visible within the plotted range of the Ag 3p core-level spectra. This is due to the fact that the corresponding splitting of the 3p states is one order of magnitude larger.

V. DISCUSSION

All results obtained by first-principles calculations are in very good agreement with experimental findings. Lattice

properties such as atomic positions, bond lengths, compressibilities, and phonon frequencies, as well as electronic properties reproduce measurements very well. All these facts are an excellent starting point for the discussion of the binding mechanism in these scheelite materials.

A first indication for the same bonding situation in both compounds are the lattice dimensions which are found to be the same. In case of ionic bonding, this would suggest that silver exhibits a very similar ionic radius as Na. Indeed, there are several indications that Ag^+ has a variable ionic radius which may vary between 0.67 Å and 1.42 Å (Refs. 35 and 36) in different compounds depending on the coordination number. Another striking fact is the A_g vibrations exhibiting the same frequencies in both compounds, thus showing that the interaction of the Ag atom with the ReO_4 tetrahedra is as little as that of Na.

In the case of $NaReO_4$, the bonding mechanism is evident. In the valence band no Na character has been detected; therefore the bonding in this material can be regarded to be completely ionic. In the case of $AgReO_4$, the strongly localized silver *d* bands and the weakly altered band structure with respect to the Na compound are strong indications of ionic behavior in $AgReO_4$. The relative oxygen contribution in the Ag bands below the Fermi level as emerging from the band-character plot is very small. The bandwidth of the O dominated band between -1.8 and -4 eV does not change when silver is introduced into the lattice. However, this band exhibits weak Ag character in $AgReO_4$. We interpret this mixed character of some bands as a polarization effect rather than covalent bonding[36] and conclude that the interaction between Ag and O is predominantly ionic. It should be noted that the rather broad bandwidth is a result of the crystal-field splitting and not of covalent bonds. Only the band dispersion of the ReO_4 bands reflects the covalent bonding inside the tetrahedra.

Also the analysis of the XPS results is consistent with a strongly ionic model of $AgReO_4$, in other words, covalent interaction due to Ag $4d$–O $2p$ mixing is not expected. The latter would yield a Ag $4d$–O $2p$ derived structure at higher binding energy which is not observed. Furthermore, it is worth noting that deformation of the outermost O *p* electron charge distribution of the anion in the crystal field of silver ions is a very important factor to understand the characteristic properties of silver salts.

To underline our hypothesis, we have further analyzed the electron density in $NaReO_4$ and $AgReO_4$ to obtain clearer indications for ionicity or covalency. In the ionic case, the electrons would be concentrated at the atomic sites and vanish in the interstitial space, whereas in the covalent situation a considerable charge density should appear in the region between the bonded atoms. The electron densities in the *M*-Re planes of $NaReO_4$ and $AgReO_4$ are depicted in Fig. 8. Clearly, there is no difference in the electron densities related to the distribution of the ReO_4 tetrahedra, another indication for the same binding mechanism. Furthermore, the electron densities have also been computed in a plane containing neighboring sodium (silver) and oxygen atoms in $NaReO_4$ ($AgReO_4$). While $NaReO_4$ does not exhibit any finite electron density in between these two atoms (Fig. 9, upper panel), a maximum electron density of 0.03 electrons per cubic a.u. ($0.20\ e/Å^3$) is found for $AgReO_4$ (Fig. 9, lower panel). This value is in close accordance with ≈ 0.01 electrons per cubic a.u. ($0.07\ e/Å^3$) in NaCl,[37] which is *the ionic textbook compound*. In conclusion, $NaReO_4$ as well as $AgReO_4$ have to be regarded as representative examples for the ionic binding mechanism.

ACKNOWLEDGMENTS

We appreciate support from the Austrian Science Fund (FWF), Projects Nos. P14004-PHY and P13430-PHY, and by the EU research and training network *EXCITING*, Contract No. HPRN-CT-2002-00317.

*Electronic address: juergen.spitaler@uni-graz.at

[1] J.E. Mayer, J. Chem. Phys. **1**, 327 (1933).
[2] L. Pauling, Phys. Today **24**, 9 (1971).
[3] W.A. Harrison, *Electronic Structure and the Properties of Solids* (Dover, New York, 1980).
[4] E. Aprá, E. Stefanovich, R. Dovesi, and C. Roetti, Chem. Phys. Lett. **186**, 329 (1991).
[5] F. Kirchhoff, J.M. Holender, and M.J. Gillan, Phys. Rev. B **49**, 17 420 (1994).
[6] A. Deb and A.K. Chatterjee, J. Phys.: Condens. Matter **10**, 11719 (1998).
[7] K. Doll and N.M. Harrison, Phys. Rev. B **63**, 165410 (2001).
[8] K. Fischer, H. Bilz, R. Haberkorn, and W. Weber, Phys. Status Solidi B **54**, 285 (1972).
[9] W.G. Kleppmann and W. Weber, Phys. Rev. B **20**, 1669 (1979).
[10] H. Kikuchi, H. Iyetomi, and A. Hasegawa, J. Phys.: Condens. Matter **10**, 11 439 (1998).
[11] H. Bilz, Cryst. Lattice Defects Amorphous Mater. **12**, 31 (1985).
[12] M. Bucher, Phys. Rev. B **30**, 947 (1984).
[13] N.C. Pyper, Philos. Trans. R. Soc. London, Ser. A **320**, 107 (1986).
[14] M. Bucher, J. Imaging Sci. **34**, 89 (1990).
[15] P. Blaha, K. Schwarz, and J. Luitz, Computer Code WIEN97 (Technische Universität Wien, Austria, 1999).
[16] J.P. Perdew and Y. Wang, Phys. Rev. B **45**, 13 244 (1992).
[17] P.E. Blöchl, O. Jepsen, and O.K. Anderson, Phys. Rev. B **49**, 16223 (1994).
[18] G. M. Sheldrick, Computer Code SHELXS-97 (University of Göttingen, Germany, 1997).
[19] G. M. Sheldrick, Computer Code SHELXL-97 (University of Göttingen, Germany, 1997).
[20] V.K. Kaushik, J. Electron Spectrosc. Relat. Phenom. **56**, 402 (1991).
[21] T. Hirono, M. Fukuma, and T. Yamada, J. Appl. Phys. **57**, 2267 (1985).
[22] E.S. Shpiro, V.I. Avaev, G.V. Antoshin, M.A. Ryashentseva, and K.M. Minachev, J. Catal. **55**, 402 (1978).
[23] R.J. Thorn, K.D. Carlson, G.W. Crabtree, and H.H. Wang, J. Phys. C **18**, 5501 (1985).
[24] P.H. Citrin and T.D. Thomas, J. Chem. Phys. **57**, 4446 (1972). In ionic systems the spacings of energy levels are independent of crystal environment and identical to those of the free ion.

[25] A. Atzersdorfer and K.J. Range, Z. Naturforsch., B: Chem. Sci. **50**, 1417 (1995).
[26] J. Beintema, Z. Kristallogr. **97**, 300 (1937).
[27] D.Y. Naumov, A.V. Virovets, S.V. Korenev, and A.I. Gubanov, Acta Crystallogr., Sect. C: Cryst. Struct. Commun. **C55**, IUC9900097 (1999).
[28] Typically the crystal volumes are underestimated by a few up to even 15%, whereas the trends in the lattice parameters are usually given reliably; R.O. Jones and O. Gunnarsson, Rev. Mod. Phys. **61**, 689 (1989).
[29] J.W. Otto, J.K. Vassiliou, R.F. Porter, and A.L. Ruoff, Phys. Rev. B **44**, 9223 (1991).
[30] J.W. Otto, J.K. Vassiliou, and R.F. Porter, J. Phys. Chem. Solids **53**, 631 (1992).
[31] Deviations up to 10% can typically still be regarded as reasonable agreement; C. Ambrosch-Draxl *et al.*, Phys. Rev. B **65**, 064501 (2002).
[32] H. Schlosser, J. Phys. Chem. Solids **53**, 855 (1992).
[33] D.K. Breitinger, L. Emmert, and W. Kress, Ber. Bunsenges. Phys. Chem. **85**, 504 (1981).
[34] Y. Abraham, N.A.W. Holzwarth, and R.T. Williams, Phys. Rev. B **62**, 1733 (2000).
[35] R. Shannon, Acta Crystallogr., Sect. A: Cryst. Phys., Diffr., Theor. Gen. Crystallogr. **32**, 751 (1976).
[36] G.S. Rohrer, *Structure and Bonding in Crystalline Materials* (Cambridge University Press, Cambridge, London, 2001).
[37] N.W. Ashcroft and N.D. Mermin, *Solid State Physics* (Saunders College Publishing, Forth Worth, 1976).
[38] R.A. Johnson, M.T. Rogers, and G.E. Leroi, J. Chem. Phys. **56**, 789 (1972).